

Design Rules for Dynamic-Template-Directed Crystallization of Conjugated Polymers

Erfan Mohammadi^{1#}, Ge Qu, Prapti Kafle, Seok-Heon Jung², Jin-Kyun Lee², Ying Diao^{1*}

¹Department of Chemical and Biomolecular Engineering, University of Illinois at Urbana–Champaign, 600 South Mathews Avenue, Urbana, Illinois 61801, United States.

²Department of Polymer Science & Engineering, Inha University, Incheon 402-751, South Korea.

SUPPORTING NOTES

Selection of ionic liquid (IL) dynamic template series. To modulate the strength of IL interaction with the conjugated polymer we have chosen three different ILs with different cations paired with TFSI anion. BMIM has an aromatic conjugated cation, PYR is a cation with non-conjugated ring and N4111 is an ammonium-based cation without a ring. The alkyl chains (methyl and butyl) and viscosities are selected to be comparable. The size of templates is decreasing in the following order: BMIM>PYR>N4111 (estimated by V_{eff} summarized in Table S1). All templating liquids should be immiscible with the polymer ink solution in chloroform during the solution coating time-frame. Moreover, the liquid-infused substrate in the AAO membrane should be energetically stable during the coating process which is validated with previously derived stability criteria¹.

Evaluating templates dynamics by estimating relative rotational relaxation time. To estimate relative rotational relaxation time (τ_{rot}) from Stokes-Einstein-Debye (SED)

hydrodynamic theory ($\tau_{rot} = \frac{3\eta V_{eff}\xi}{k_B T}$), we used literature values of viscosity (η) and the effective molecular volume (V_{eff}) (Table S1). We assumed that ξ is comparable across all liquids. The estimated τ_{rot} values relative to ethylene glycol are summarized in Table S1.

Template	GLY	EG	N4111	PYR	BMIM
η (mPa.s)	1412 ²	20 ³	116 ⁴	70 ⁵	52 ⁶
V_{eff} (Å ³)	100 ⁷	121 ^(a)	122 ⁸	166 ⁹	200 ¹⁰
Relative τ_{rot}	54	1	6	5	4

Table S1. Rough estimation of relative orientational relaxation time of investigated templates at

20°C. ^(a)Estimated from molecular volume.

SUPPORTING FIGURES

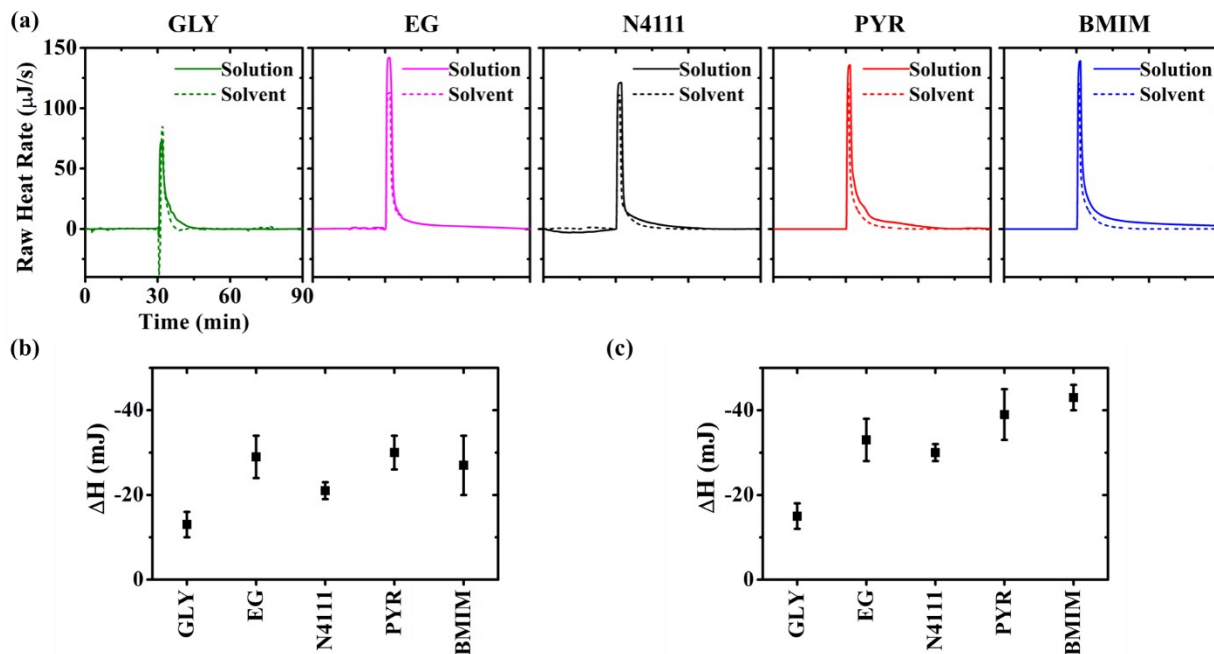


Figure S1. Single-injection isothermal titration calorimetry (S-IITC) for quantifying interaction between templates and conjugated polymer. During S-IITC, we titrated solution or solvent over 50 μL of the liquid templates. (a) Heat rate data from a single injection of 3 μL of solution (solid line) and solvent (dashed line) on 50 μL pure liquid templates. Cumulative enthalpy is obtained by calculating the area under each peak after subtracting the dilution or mechanical effects. At least 3 repeat injections were used to calculate the enthalpy. (b) Chloroform (solvent) and (c) DPP-BTz solution titration enthalpy change per injection. We obtained the net interaction enthalpy between DPP-BTz and liquid templates from measuring the difference in the heat released at constant pressure during titrating the DPP-BTz solution and the neat solvent.

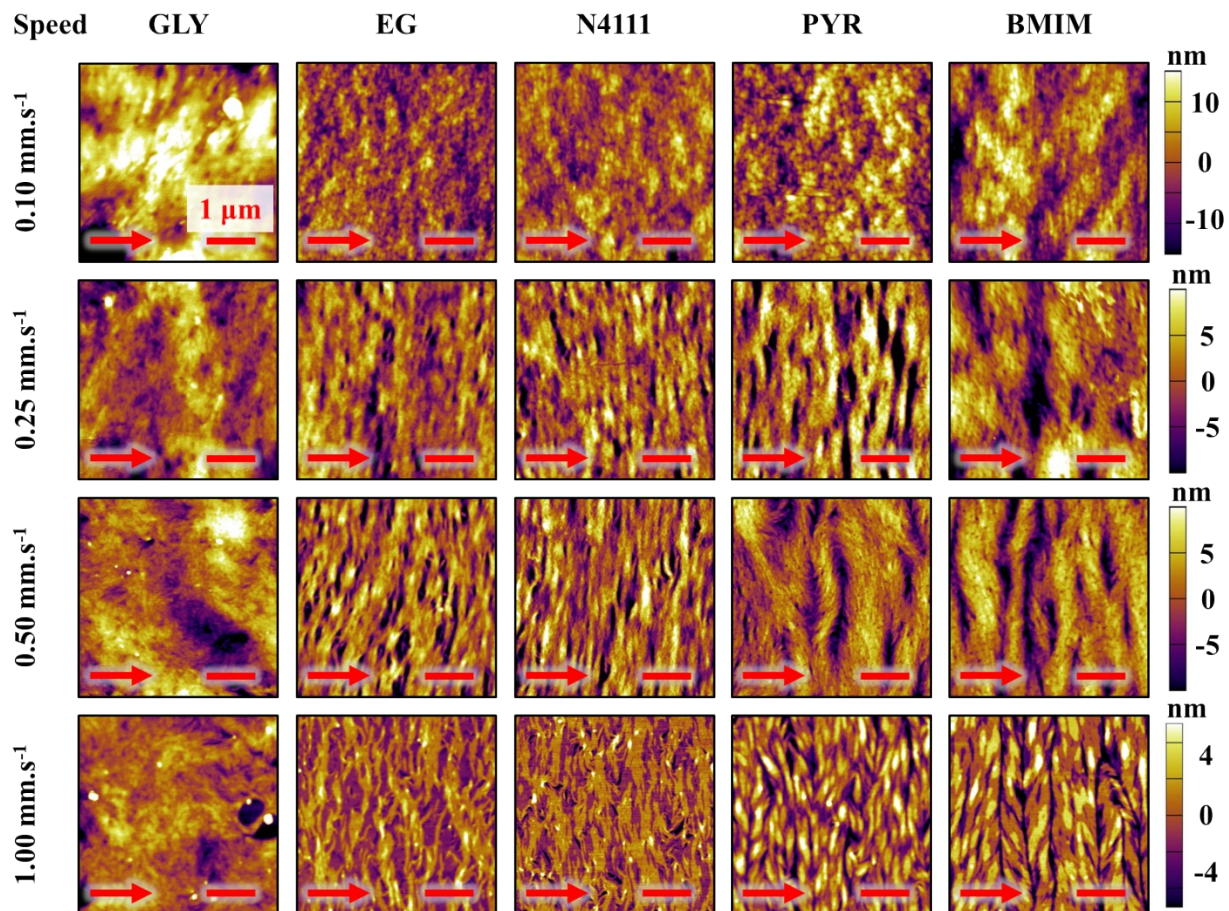


Figure S2. Meso-scale morphology of DPP-BTz films as a function of templating substrate and coating speed. Tapping-mode AFM height images with 1 μm scale bars. The arrow indicates the coating direction.

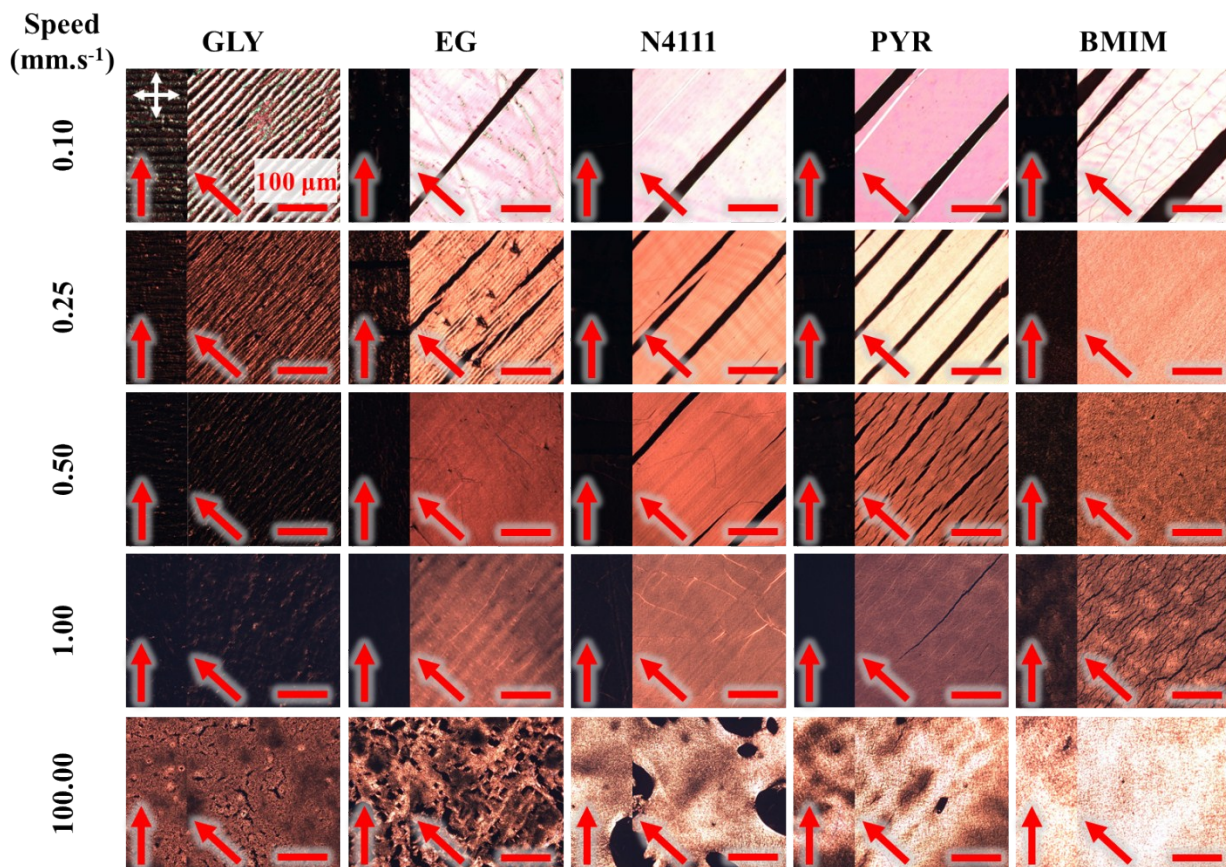


Figure S3. CPOM images of DPP-BTz films as a function of templating substrate and coating speed.

Cross-polarized optical microscopy images of CP films as a function of substrate and coating speed.

Polarizers orientation is shown as white crossed arrows and the red single arrows show the coating direction

(all scale bars are 100 μm). When sample illuminates upon rotating the stage, film is uniaxially aligned and

when the contrast is negligible polymer chains are isotropic.

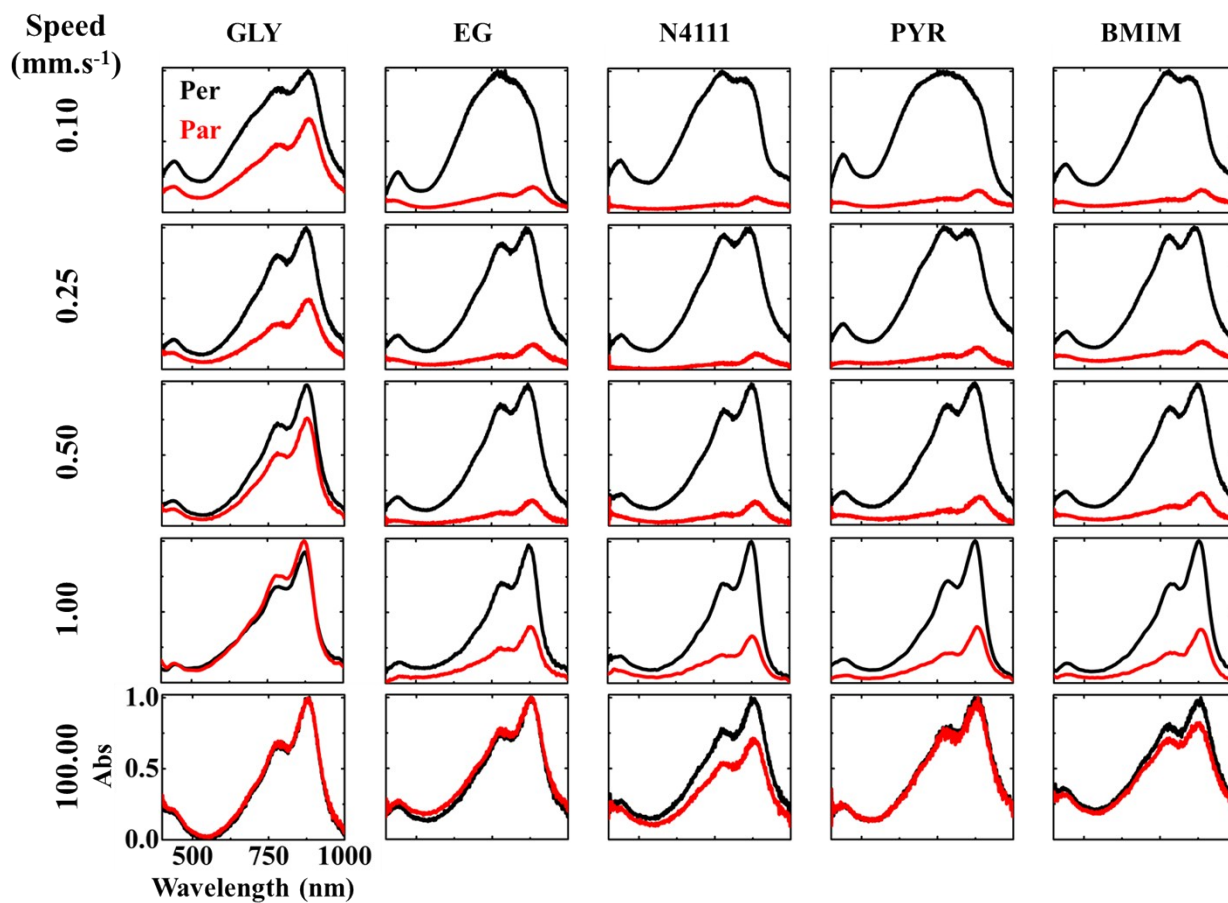


Figure S4. Quantifying macroscale alignment of DPP-BTz thin films. Normalized absorption spectra of polarized UV-vis spectroscopy when polymer film coating direction is parallel (red) and perpendicular (black) with respect to the polarizer axis. The substantial change in polymer chain alignment and vibronic ratio as a function of substrate and speed is discernable.

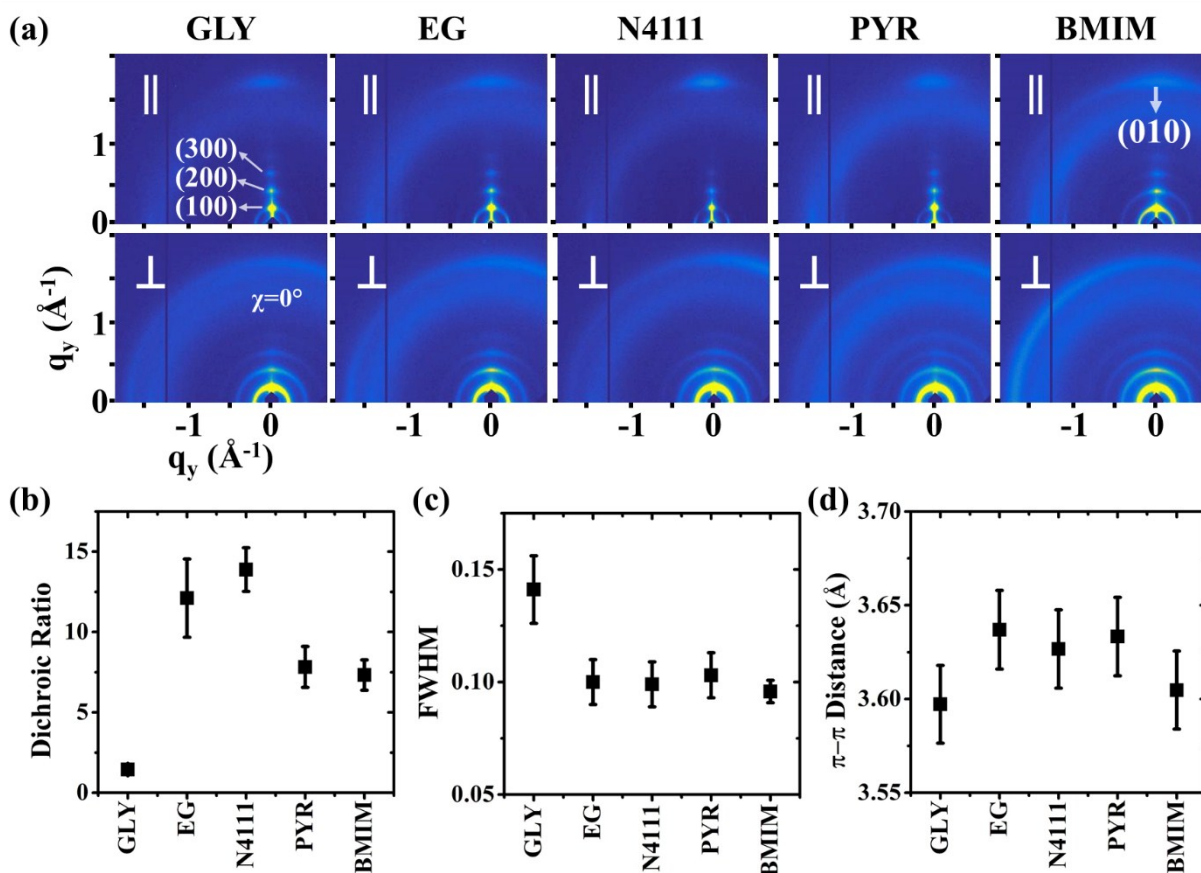


Figure S5. GIXD analysis of DPP-BTz thin films coated on various substrates at 0.1 mm.s^{-1} . (a) GIXD micrographs of DPP-BTz thin films coated on various templates with the incident beam oriented parallel (\parallel) ($\varphi=0^\circ$) and perpendicular (\perp) ($\varphi=90^\circ$) to the coating direction. (b) GIXD dichroic ratio (R_{GIXD}) calculated from analyzing edge-on π - π stacking peaks perpendicular and parallel to the coating direction. (c) FWHM of "edge-on" π - π stacking peak and (d) π - π stacking distance for DPP-BTz polymer thin films coated on various templates.

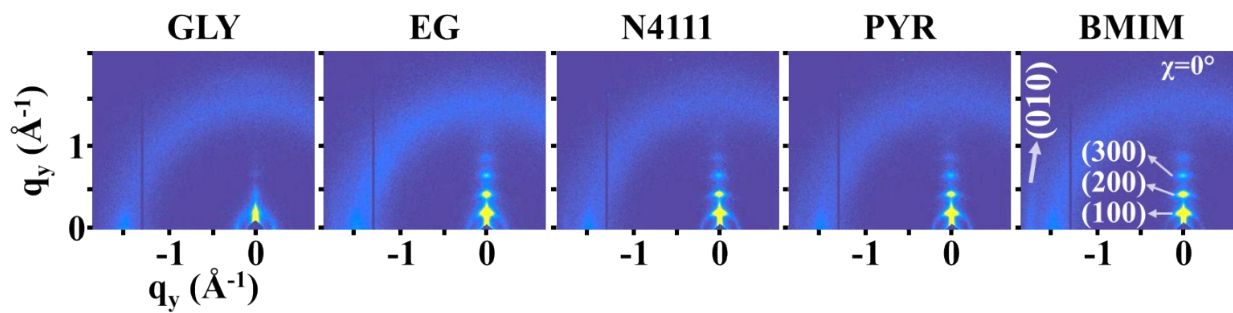


Figure S6. GIXD micrographs of DPP-BTz thin films coated on various substrates at 100 mm.s⁻¹.

Beam orientation is irrelevant since films are isotropic proved by UV-vis and C-POM morphology analysis.

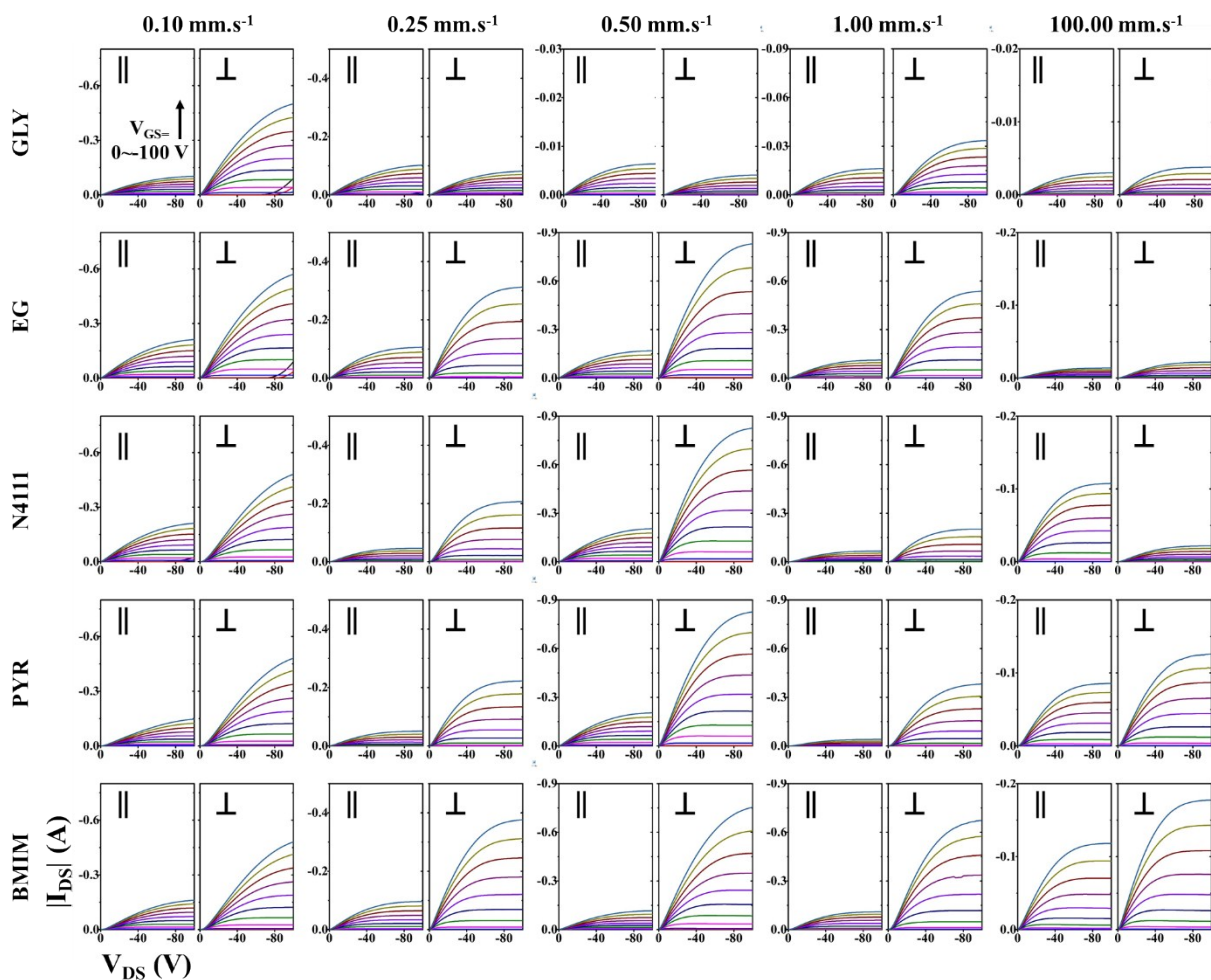


Figure S7. DPP-BTz thin film field-effect transistor output characteristics. Output curves of films coated on various templates. The coating speed is varied from 0.10 to 100.00 $\text{mm}\cdot\text{s}^{-1}$ but the film thickness is being fixed by changing solution concentration. DPP-BTz films were transferred to OTS-treated SiO_2 and BGTC structure was fabricated by thermally depositing MoO_3/Ag electrodes atop ($W = 840 \mu\text{m}$, $L = 47 \mu\text{m}$).

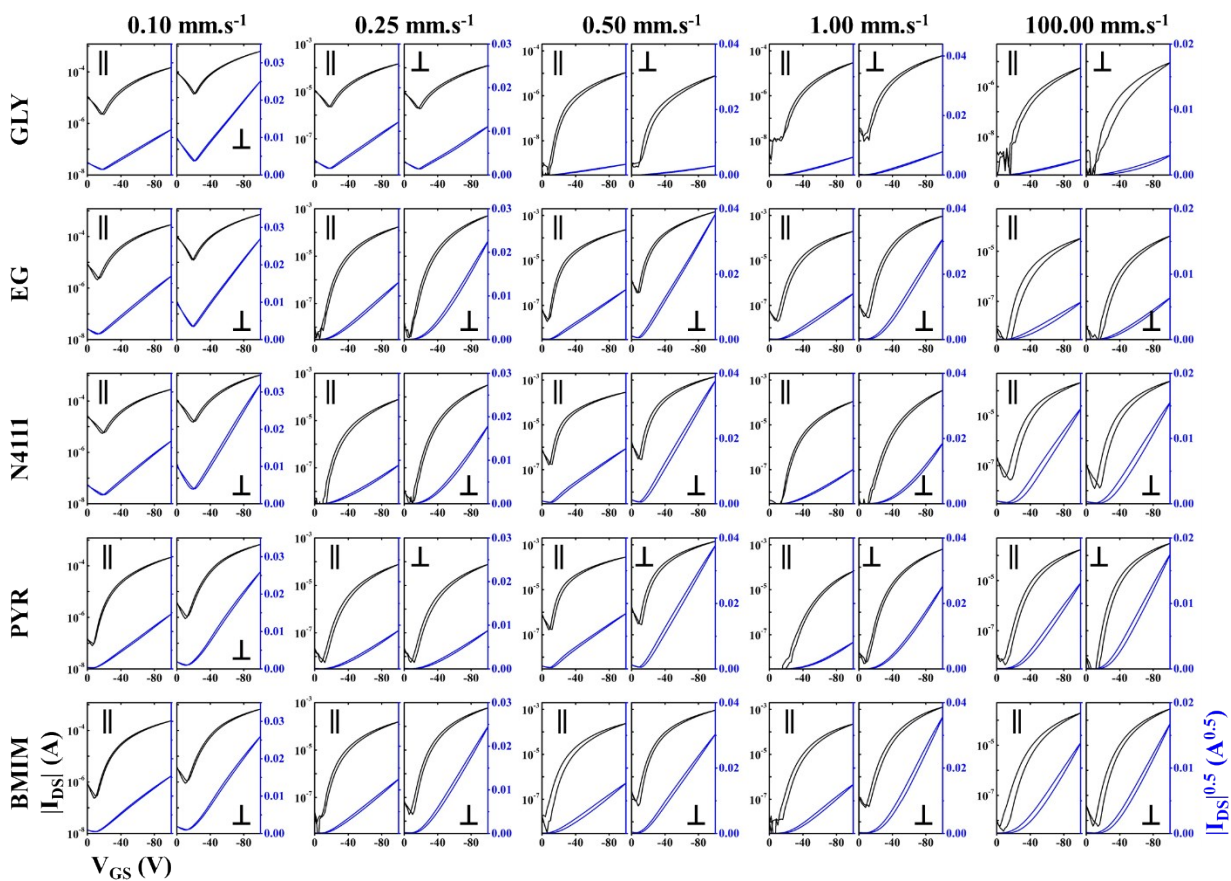


Figure S8. DPP-BTz thin film field-effect transistor transfer characteristics. Source-drain voltage for is fixed at -100 V. Carrier transport is measured parallel and perpendicular to the coating direction. Transfer curves are nearly ideal with the square root of source-drain current being linear for almost all conditions.

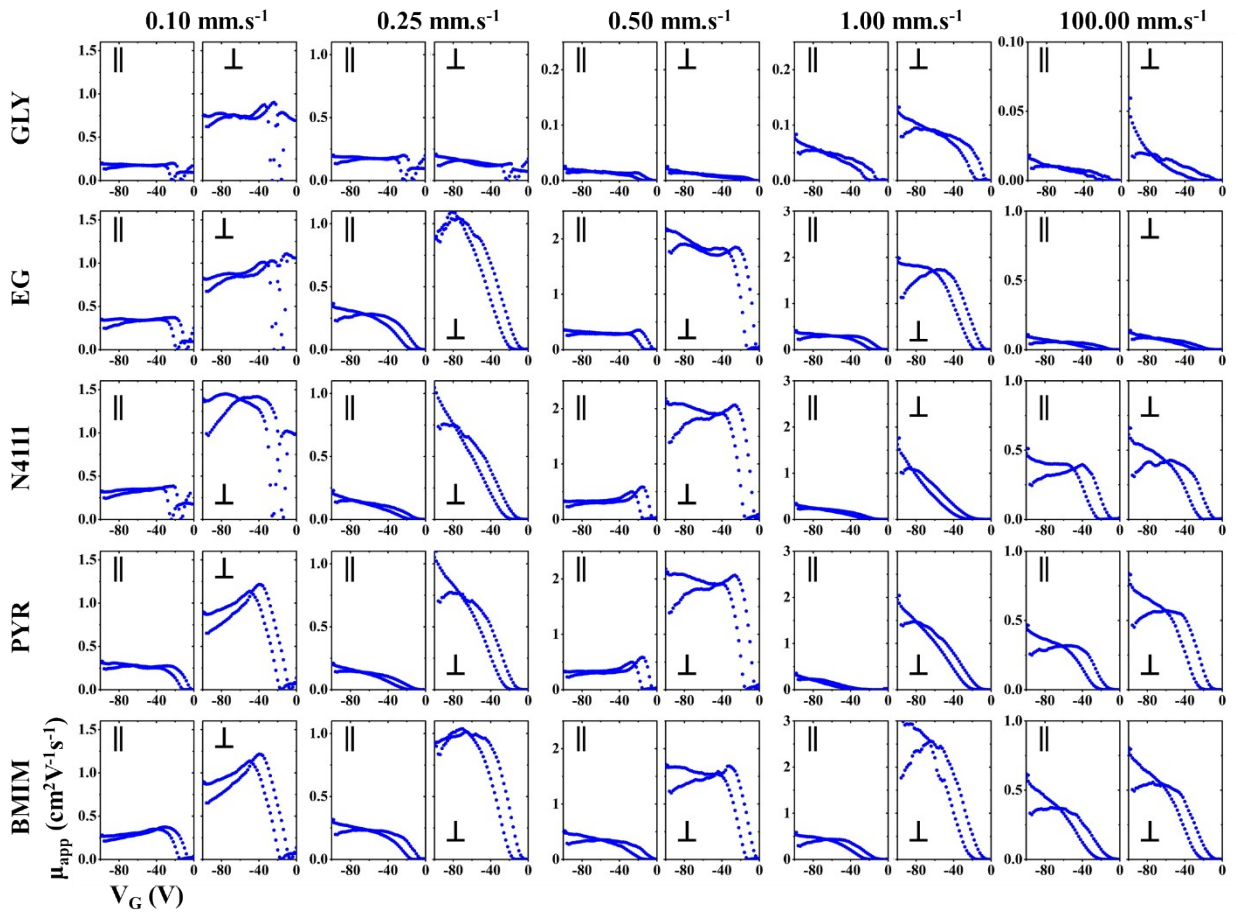


Figure S9. DPP-BTz thin film field-effect transistor transfer characteristics.

REFERENCES

1. Mohammadi, E.; Zhao, C.; Meng, Y.; Qu, G.; Zhang, F.; Zhao, X.; Mei, J.; Zuo, J.-M.; Shukla, D.; Diao, Y., Dynamic-template-directed multiscale assembly for large-area coating of highly-aligned conjugated polymer thin films. *Nat. Commun.* **8**, 16070 (2017).
2. Segur, J. B.; Oberstar, H. E., Viscosity of Glycerol and Its Aqueous Solutions. *Ind. Eng. Chem. Res.* **43**, 2117-2120 (1951).
3. Ethylene Glycol. In *Ullmann's Encyclopedia of Industrial Chemistry*.
4. McFarlane, D. R.; Sun, J.; Golding, J.; Meakin, P.; Forsyth, M., High conductivity molten salts based on the imide ion. *Electrochim. Acta* **45**, 1271-1278 (2000).
5. Hajime, M.; Masahiro, Y.; Kazumi, T.; Masakatsu, N.; Yukiko, K.; Yoshinori, M., Highly Conductive Room Temperature Molten Salts Based on Small Trimethylalkylammonium Cations and Bis(trifluoromethylsulfonyl)imide. *Chem. Lett.* **29**, 922-923 (2000).
6. Bonhôte, P.; Dias, A.-P.; Papageorgiou, N.; Kalyanasundaram, K.; Grätzel, M., Hydrophobic, Highly Conductive Ambient-Temperature Molten Salts. *Inorg. Chem.* **35**, 1168-1178 (1996).
7. Banerjee, D.; Bhat, S. V., Vitrification, relaxation and free volume in glycerol–water binary liquid mixture: Spin probe ESR studies. *J. Non-Cryst. Solids* **355**, 2433-2438 (2009).
8. Strauch, M.; Bónsa, A.-M.; Golub, B.; Overbeck, V.; Michalik, D.; Paschek, D.; Ludwig, R., Deuteron quadrupole coupling constants and reorientational correlation times in protic ionic liquids. *Phys. Chem. Chem. Phys.* **18**, 17788-17794 (2016).
9. Alam, T. M.; Dreyer, D. R.; Bielawski, C. W.; Ruoff, R. S., Combined Measurement of Translational and Rotational Diffusion in Quaternary Acyclic Ammonium and Cyclic Pyrrolidinium Ionic Liquids. *J. Phys. Chem. B* **117**, 1967-1977 (2013).
10. Hunger, J.; Stoppa, A.; Schrödle, S.; Hefter, G.; Buchner, R., Temperature Dependence of the Dielectric Properties and Dynamics of Ionic Liquids. *ChemPhysChem* **10**, 723-733 (2009).